Monthly Notices
of the
ROYAL ASTRONOMICAL SOCIETY

MNRAS **437,** 2307–2319 (2014)
Advance Access publication 2013 November 21

doi:10.1093/mnras/stt2047

The VMC Survey – VIII. First results for anomalous Cepheids*

V. Ripepi,[1]† M. Marconi,[1] M. I. Moretti,[1] G. Clementini,[2] M.-R. L. Cioni,[3,4]‡ R. de Grijs,[5,6] J. P. Emerson,[7] M. A. T. Groenewegen,[8] V. D. Ivanov[9] and J. M. Oliveira[10]

[1]*INAF-Osservatorio Astronomico di Capodimonte, via Moiariello 16, I-80131 Naples, Italy*
[2]*INAF-Osservatorio Astronomico di Bologna, via Ranzani 1, I-40127 Bologna, Italy*
[3]*School of Physics, Astronomy and Mathematics, University of Hertfordshire, Hatfield AL10 9AB, UK*
[4]*Leibnitz-Institut für Astrophysik Potsdam, An der Sternwarte 16, D-14482 Potsdam, Germany*
[5]*Kavli Institute for Astronomy and Astrophysics, Peking University, Yi He Yuan Lu 5, Hai Dian District, Beijing 100871, China*
[6]*Department of Astronomy, Peking University, Yi He Yuan Lu 5, Hai Dian District, Beijing 100871, China*
[7]*Astronomy Unit, School of Physics & Astronomy, Queen Mary University of London, Mile End Road, London E1 4NS, UK*
[8]*Koninklijke Sterrenwacht van België, Ringlaan 3, B-1180, Brussel, Belgium*
[9]*European Southern Observatory, Ave. Alonso de Cordova 3107, Casilla 19, Chile*
[10]*Astrophysics Group, Lennard-Jones Laboratories, Keele University, Staffordshire ST5 5BG, UK*

Accepted 2013 October 21. Received 2013 September 27; in original form 2013 May 2

ABSTRACT

The VISTA near-infrared YJK_s survey of the Magellanic Clouds System (VMC, PI M.-R. L. Cioni) is collecting deep K_s-band time-series photometry of the pulsating variable stars hosted in the system formed by the two Magellanic Clouds and the Bridge connecting them. In this paper, we present for the first time K_s-band light curves for anomalous Cepheid (AC) variables. In particular, we have analysed a sample of 48 Large Magellanic Cloud ACs, for which identification and optical magnitudes were obtained from the OGLE III and IV catalogues. The VMC K_s-band light curves for ACs are well sampled, with the number of epochs ranging from 8 to 16, and allowing us to obtain very precise mean K_s magnitudes with errors on average of the order of 0.01 mag. The $\langle K_s \rangle$ values were used to build the first period–luminosity and period–Wesenheit relations in the near-infrared for fundamental mode and first overtone ACs. At the same time we exploited the optical (V, I) OGLE data to build accurate period–luminosity, period–luminosity–colour and period–Wesenheit relations both for fundamental mode and first overtone ACs. For the first time, these relations were derived from a sample of pulsators which uniformly cover the whole AC instability strip. The application of the optical period–Wesenheit relation to a sample of dwarf galaxies hosting a significant population of ACs revealed that this relation is a valuable tool for deriving distances within the Local Group. Due to its lower dispersion, we expect the K_s period–Wesenheit relations first derived in this paper to represent a valuable tool for measuring accurate distances to galaxies hosting ACs when more data in near-infrared filters become available.

Key words: surveys – stars: variables: Cepheids – galaxies: distances and redshifts – Magellanic Clouds.

1 INTRODUCTION

The Magellanic Clouds (MCs) play a fundamental role in the context of stellar populations and galactic evolution studies (see e.g. Harris & Zaritsky 2004, 2009). Together with the Milky Way they form the closest example of ongoing complex interaction among galaxies (see e.g. Putman et al. 1998; Muller et al. 2004; Stanimirović, Staveley-Smith & Jones 2004; Bekki & Chiba 2007; Venzmer, Kerp & Kalberla 2012; For, Staveley-Smith & McClure-Griffiths 2013). Moreover, since they are more metal poor than our Galaxy and host a significant population of younger populous clusters, the MCs represent an ideal laboratory for testing physical and numerical assumptions of stellar evolution codes (see e.g. Matteucci et al. 2002; Brocato et al. 2004; Neilson & Langer 2012).

*Based on observations made with VISTA at ESO under programme ID 179.B-2003.

† E-mail: ripepi@oacn.inaf.it
‡ Research Fellow of the Alexander von Humboldt Foundation.

In the framework of the extragalactic distance scale, the Large Magellanic Cloud (LMC) represents the first crucial step on which the calibration of classical Cepheid (CC) period–Luminosity (*P–L*) relations and in turn of secondary distance indicators relies (see e.g. Freedman et al. 2001; de Grijs 2011; Riess et al. 2011; Walker 2012, and references therein). Similarly, the LMC hosts several thousand RR Lyrae variables, which represent the most important Population II standard candles through the well-known M_V(RR)–[Fe/H] and near-infrared (NIR) metal-dependent *P–L* relations. Hence, the LMC is the ideal place to compare the distance scales derived from Population I and II indicators (see e.g. Clementini et al. 2003; Walker 2012, and references therein).

In this context, NIR observations of pulsating stars (see e.g. Ripepi et al. 2012a; Moretti et al. 2013, and references therein) are very promising. Such observations over the whole Magellanic system, including the relatively unexplored Bridge connecting the two Clouds, represent one of the most important aims of the *VISTA near-infrared YJK$_s$ survey of the Magellanic Clouds system* (VMC; Cioni et al. 2011, hereinafter Paper I). The VMC ESO public survey is acquiring deep NIR photometric data in the *Y*, *J* and K_s filters on a wide area across the Magellanic system, with the VIRCAM camera (Dalton et al. 2006) of the ESO VISTA telescope (Emerson, McPherson & Sutherland 2006). The principal scientific aims of VMC are the reconstruction of the spatially resolved star formation history (SFH) and the determination of the 3D structure of the whole Magellanic system. The observational strategy, planned to go as deep as $K_s \sim 20.3$ mag (Vega) at signal-to-noise ratio (S/N) = 10, will allow us to detect sources encompassing most phases of stellar evolution, namely the main-sequence, the subgiant branch, the upper and lower red giant branch (RGB), the red clump, the RR Lyrae and Cepheid location, the asymptotic giant branch (AGB), the post-AGB and planetary nebulae phases, but also supernova remnants, etc. These different stellar populations will allow us to study age and metallicity distributions within the whole MC system.

The properties of the CCs and RR Lyrae stars observed by the VMC survey are addressed by Ripepi et al. (2012a,b). In these papers, the authors provide important results on the calibration of the distance scales for both these important standard candles. Beyond these two classes of variables, other kinds of pulsating stars play an important role both as distance indicators and as stellar population tracers. In particular, anomalous Cepheids (ACs) are Population II stars, according to their low metallicity, with periods shorter than 2 d and brighter than RR Lyrae stars by an amount that typically ranges from 0.3 mag for the shortest period to 2 mag for the longest period pulsators (see e.g. Caputo 1998; Caputo et al. 2004; Marconi, Fiorentino & Caputo 2004, and references therein). From the evolutionary point of view, these variables are usually associated with the central He burning phase of stars with masses from $\sim$1.3 to $\sim$2.1 $M_\odot$ and metallicities lower than $Z = 0.0004$ ([Fe/H] ≈ -1.7 dex, for $Z_\odot = 0.02$) (see Caputo 1998; Marconi et al. 2004, for details). In this low-metallicity regime, the zero-age horizontal branch (ZAHB) is predicted to show a turnover at lower effective temperatures. Indeed, as the mass increases along the ZAHB, the effective temperature decreases down to a minimum value beyond which both the effective temperature and the luminosity increase up to the values corresponding to the transition mass limit (see e.g. Caputo 1998, for details). Above this limit, the star ignites the triple-α reaction quiescently and burns central Helium along the blue loop phase, becoming a CC when crossing the instability strip. The location of the ACs in a period magnitude plane is therefore the downward extension of the distribution of metal-poor CCs, and in the short period range the discrimination between the two classes can be risky, as extensively discussed in Caputo et al. (2004). These authors have also demonstrated that both the predicted limiting magnitude for massive pulsators and the magnitude of RR Lyrae stars, depend on the assumed metallicity, with the difference between these magnitudes increasing with the metal content.

In the LMC, there are 86 ACs (Soszyński et al. 2008, 2012). An investigation of the properties of these pulsators in the optical bands has been recently presented by Fiorentino & Monelli (2012), using these objects as stellar population tracers. These authors derived pulsation constraints on their mode identification and mass estimate. Nevertheless, optical period–luminosity–colour (*P–L–C*) and Wesenheit (*P–W*) relations (see Madore 1982; Madore & Freedman 1991, for a detailed discussion) for the LMC ACs are still lacking in the literature. These relations are important tools providing an alternative and independent estimate of the distance to the LMC. Furthermore, for the reasons discussed above, we expect significant advantages when deriving similar relations in the NIR bands.

The VMC data for the ACs are presented in Section 2. The *P–L*, *P–W* and *P–L–C* relations in the optical (on the basis of the OGLE data) and in the NIR (on the basis of the VMC data) derived for fundamental-mode (F) and first overtone (FO) ACs are discussed in Sections 3 and 4. The zero-point calibrations of the AC *P–L*, *P–W* and *P–L–C* relations and their application are presented in Section 5. Finally, a summary of the main results is presented in Section 6.

2 ACS IN THE VMC SURVEY

ACs in the LMC were identified and characterized in the optical bands by Soszyński et al. (2008, and references therein) as part of the OGLE III project.[1] For the LMC tile 8_8 [including the South Ecliptic Pole (SEP)] which lies outside the area imaged by OGLE III, we used results of an early release of stage IV of the OGLE survey (Soszyński et al. 2012). In these surveys, a total of 86 ACs were found (83 by OGLE III and 3 by OGLE IV), of which 66 are F and 20 are FO pulsators.

In this paper, we present results for the ACs included in 11 'tiles' (1.5 deg^2) completely or nearly completely observed, processed and catalogued by the VMC survey as of 2013 March, namely the tiles LMC 4_8, 5_3, 5_5, 5_7, 6_4, 6_5, 6_6, 6_8, 7_3, 7_5 and 8_8 (see Fig. 1). Tile LMC 6_6 is centred on the well-known 30 Dor star-forming region, tiles LMC 5_5, 6_4 and 6_5 are placed on the bar of the LMC, whereas the remaining tiles lie in less crowded regions of the galaxy. We note that tile LMC 8_8 encompasses the SEP which will be observed by the *Gaia* satellite during its commissioning phase (Lindegren & Perryman 1996; Lindegren 2010).

The general observing strategy of the VMC survey is described in detail in Paper I, whereas the procedures specifically applied to the variable stars can be found in Moretti et al. (2013). Here, we only recall that to obtain well-sampled light curves, the VMC K_s-band time series observations were scheduled in 12 separate epochs distributed ideally over several consecutive months. The VMC data, processed through the pipeline (Irwin et al. 2004) of the VISTA Data Flow System (Emerson et al. 2004) are in the VISTA photometric system (Vegamag = 0). The time series photometry used in this paper was retrieved from the VISTA Science Archive (VSA; Cross

[1] http://ogle.astrouw.edu.pl

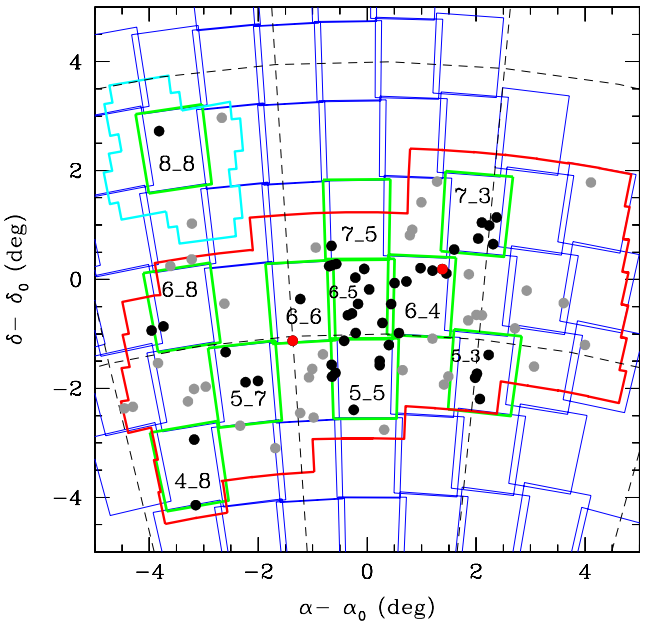

Figure 1. Distribution of the known ACs over the LMC (projected in the sky adopting $\alpha_0 = 81\overset{\circ}{.}0$ and $\delta_0 = -69\overset{\circ}{.}0$). Grey and black filled circles show the ACs observed by OGLE and those falling in the VMC tiles considered in this paper, respectively. The red filled circles represent the only two stars without a VMC counterpart within 1.0 arcsec (see text). Thin blue and thick green squares (distorted by the projection into the sky) show part of the VMC tiles in the LMC and the 11 tiles treated in this paper, respectively. The thick red and light blue lines show the areas covered by OGLE III and IV (released up to now), respectively.

Table 1. Number of ACs in the 11 VMC tiles analysed in this paper according to OGLE III/IV.

Tile LMC	RA (centre) J(2000)	Dec. (centre) J(2000)	#ACs	Epochs (VMC)	OGLE
4_8	06:06:32.95	−72:08:31.2	2	10	III
5_3	04:58:11.66	−70:35:28.0	4	11	III
5_5	05:24:30.34	−70:48:34.2	8	15	III
5_7	05:51:04.87	−70:47:31.2	3	8	III
6_4	05:12:55.80	−69:16:39.4	8	14	III
6_5	05:25:16.27	−69:21:08.3	10	9	III
6_6	05:37:40.01	−69:22:18.1	3	14	III
6_8	06:02:21.98	−69:14:42.4	2	14	III
7_3	05:02:55.20	−67:42:14.8	6	16	III
7_5	05:25:58.44	−67:53:42.0	1	14	III
8_8	05:59:23.14	−66:20:28.7	1	16	IV

et al. 2012).[2] For our analysis, we used the VMC data acquired until the end of 2013 March.

According to OGLE III/IV, 48 ACs are expected to lie in the 11 tiles analysed in this paper. Fig. 1 and Table 1 show the distribution of such stars in the VMC tiles. The OGLE III and IV catalogues of ACs were cross-correlated against the VMC catalogue to obtain the K_s light curves for these variables.

All but one of the 48 ACs were found to have a counterpart in the VMC catalogue (see Table 2). The only object without VMC counterpart in the VSA within 3 arcsec (see Fig. 2) is OGLE-LMC-ACEP-024, which is expected to fall well within the tile LMC 6_4. This star has a luminosity $I = 17.679$ mag and $V = 17.986$ mag and no remarks in the OGLE III catalogue. There is a match if we enlarge the pairing radius to 5 arcsec, but the corresponding star is clearly too bright ($K_s \sim 12.8$ mag). An inspection of the VMC image reveals that the star is placed in the outskirts of the cluster NGC 1252 in a rather crowded region. This could explain the lack of a detection. For one of the objects with VMC identification, i.e. OGLE-LMC-ACEP-065 in tile LMC 6_6, the VSA data base did not return any time series data. This is likely because the star is located at the very edge of the frame, where the sensitivity is low and the target cannot be detected in the single-epoch frames. Looking in more detail at this object on the VMC image (see Fig. 2), it appears that some crowding is present but the target should be easily detected at least in the neighbour tile LMC 5_6 which was not observed yet.

As shown in Table 2, the sample of ACs discussed here includes 36 F- and 10 FO-mode pulsators. This sample represents more than 50 per cent of the total number of ACs in the LMC. The VMC time series K_s photometry for these 46 objects is provided in Table 3, which is published in its entirety in the online version of the paper.

Periods and epochs of maximum light available from the OGLE III catalogue were used to fold the K_s-band light curves produced by the VMC observations. The OGLE IV catalogue provides only the period for the AC LMC571.05.5070; hence, we obtained the Epoch of maximum from the analysis of the star V-band light curve. The K_s-band light curves for a sample of 42 ACs with useful light curves are shown in Figs 3 and 4. Apart from a few cases, these light curves are generally well sampled and nicely shaped. Intensity-averaged $\langle K_s \rangle$ magnitudes were derived from the light curves simply using custom software written in C, that performs a spline interpolation to the data with no need of using templates. Some evidently discrepant data points in the light curves were excluded from the fit but were plotted in the figure for completeness (note that most of these 'bad' data points belong to observations collected during nights that did not strictly meet the VMC quality criteria). The final spline fit to the data is shown by a solid line in Figs 3 and 4. Final $\langle K_s \rangle$ magnitudes are provided in Table 4.

Four objects in our sample were excluded, namely OGLE-LMC-ACEP-011, 039, 042, 067. Their light curves are displayed in Fig. 5, whereas their finding charts are shown in Fig. 2. A quick analysis of the finding charts reveals that all these stars have significant problems of crowding/blending (particularly, star 011).

It is important to remember that all the K_s photometry presented in this paper is in the VISTA system. To make it easy to compare our results with the widely used 2MASS system, we note that the two systems are very close to each other. In particular, the VMC K_s magnitude depends only mildly on the $(J - K_s)$ colour. Indeed, the empirical results available to date[3] show that: $(J - K_s)(2MASS) = 1.081(J-K_s)(VISTA)$ and $K_s(2MASS) = K_s(VISTA) - 0.011(J-K_s)(VISTA)$. Unfortunately, for the majority of our targets, we only have a few J measurements (four phase points); hence, a star-by-star correction based on the $(\langle J \rangle - \langle K_s \rangle)$ colour is likely to introduce larger errors than the correction itself. Furthermore, since the measured $(\langle J \rangle - \langle K_s \rangle)$ of our AC sample

[2] http://horus.roe.ac.uk/vsa/

[3] http://casu.ast.cam.ac.uk/surveys-projects/vista/technical/photometric-properties

Table 2. Cross-identification and main characteristics of the ACs in the 11 'tiles' analysed in this paper. The columns report: (1) OGLE identification, (2) right ascension (OGLE), (3) declination (OGLE), (4) mode of pulsation, (5) period, (6) epoch of maximum light, (7) intensity-averaged I magnitude (OGLE), (8) intensity-averaged V magnitude (OGLE), (9) VMC identification, (10) VMC tile, (11) number of K_s epochs and (12) notes on individual stars.

ID	RA (J2000)	Dec. (J2000)	M	Period (d)	Epoch (d)	$\langle I \rangle$ (mag)	$\langle V \rangle$ (mag)	VMC-ID	Tile	$n_{\rm Epochs}$	Notes
(1)	(2)	(3)	(4)	(5)	(6)	(7)	(8)	(9)	(10)	(11)	(12)
OGLE-LMC-ACEP-035	5:18:22.19	−69:03:38.4	FO	0.446 049	52 115.883 31	18.143	18.658	558355019633	6_4	14	
OGLE-LMC-ACEP-013	4:59:56.62	−70:42:24.9	FO	0.500 923	52 166.709 18	17.963	18.488	558359106778	5_3	11	
OGLE-LMC-ACEP-043	5:24:35.40	−68:48:22.6	FO	0.506 47	52 167.591 35	17.913	18.593	558356009732	6_5	9	
OGLE-LMC-ACEP-028	5:13:10.02	−68:46:11.9	FO	0.599 253	50 457.564 27	17.574	18.322	558354835825	6_4	14	a
OGLE-LMC-ACEP-068	5:51:09.02	−70:45:42.6	F	0.625 645	52 194.189 81	18.265	18.809	558360489508	5_7	8	
OGLE-LMC-ACEP-049	5:28:03.58	−69:39:15.2	F	0.644 796	52 167.329 17	18.011	18.451	558356666394	6_5	9	
OGLE-LMC-ACEP-071	5:54:43.24	−70:10:16.1	FO	0.676 209	52 187.358 69	17.330	17.755	558360071488	5_7	8	
OGLE-LMC-ACEP-045	5:26:24.68	−68:57:55.0	F	0.678 431	52 167.432 89	18.325	18.976	558356105371	6_5	9	
OGLE-LMC-ACEP-051	5:30:14.23	−68:42:31.1	F	0.708 606	52 167.2697	18.200	18.845	558355948009	6_5	9	
OGLE-LMC-ACEP-023	5:07:52.42	−68:50:28.8	FO	0.723 433	50 726.2685	17.194	17.763	558354917807	6_4	14	
OGLE-LMC-ACEP-034	5:17:11.15	−69:58:33.1	F	0.734 298	52 123.775 57	17.874	18.474	558355708277	6_4	14	
OGLE-LMC-ACEP-008	4:58:24.59	−71:05:11.5	FO	0.749 068	52 166.141 21	17.300	17.911	558359341685	5_3	11	
OGLE-LMC-ACEP-024	5:08:44.05	−68:46:01.2	F	0.794 464	50 726.768 49	17.679	17.986	558354864345	6_4	0	b
OGLE-LMC-ACEP-009	4:58:51.29	−67:44:23.9	FO	0.800 08	52 166.342 28	17.344	17.913	558351428166	7_3	16	
OGLE-LMC-ACEP-081	6:09:38.40	−69:34:04.1	F	0.800 838	52 194.399 49	17.917	18.504	558354433783	6_8	14	
OGLE-LMC-ACEP-067	5:48:22.08	−70:45:49.3	F	0.820 921	52 168.845 04	17.786	18.451	558360481966	5_7	7	c
OGLE-LMC-ACEP-010	4:59:00.10	−68:14:01.1	F	0.834 201	52 166.341 25	18.068	18.723	558351741077	7_3	16	
OGLE-LMC-ACEP-078	6:06:58.20	−72:52:08.7	FO	0.856 556	52 187.113 24	16.979	17.417	558367620049	4_8	10	
OGLE-LMC-ACEP-041	5:21:14.35	−70:29:39.5	F	0.878 142	50 831.148 18	17.625	18.200	558361532603	5_5	15	
OGLE-LMC-ACEP-063	5:37:54.39	−69:19:28.7	F	0.893 031	52 187.443 48	18.013	18.756	558357554473	6_6	14	
OGLE-LMC-ACEP-007	4:57:31.48	−70:15:53.6	F	0.896 399	52 166.184 52	17.688	18.247	558358821009	5_3	11	
OGLE-LMC-ACEP-017	5:02:03.13	−68:09:30.4	F	0.929 995	52 166.078 49	17.585	18.190	558351666932	7_3	16	
OGLE-LMC-ACEP-040	5:21:13.22	−70:34:20.7	F	0.960 577	50 831.323 86	17.433	18.037	558361590075	5_5	15	
OGLE-LMC-ACEP-054	5:31:06.72	−68:22:29.8	F	0.980 222	52 167.478 34	17.901	18.798	558353586650	7_5	14	
OGLE-LMC-ACEP-039	5:20:44.47	−69:47:46.5	F	0.992 407	50 455.256 98	17.660	18.245	558356832178	6_5	9	c
OGLE-LMC-ACEP-011	4:59:38.09	−70:37:45.5	F	0.998 59	51 999.6182	17.671	18.254	558359538067	5_3	3	c
OGLE-LMC-ACEP-050	5:28:57.71	−70:07:15.5	FO	1.044 691	50 454.749 62	16.609	17.049	558361189093	5_5	15	
OGLE-LMC-ACEP-042	5:23:34.60	−69:10:58.2	F	1.079 036	52 167.369 92	17.897	18.715	558356267143	6_5	5	c
LMC571.05.5070	6:01:41.77	−65:58:53.5	F	1.087 061	55 557.824 71	17.181	17.686	558349409852	8_8	16	
OGLE-LMC-ACEP-077	6:04:35.73	−71:40:35.8	F	1.122 498	52 187.660 68	17.459	18.099	558367137280	4_8	10	
OGLE-LMC-ACEP-056	5:31:49.45	−70:33:22.6	F	1.124 003	52 167.636 76	17.284	17.877	558361558150	5_5	15	
OGLE-LMC-ACEP-079	6:07:02.01	−69:31:55.2	F	1.155 17	52 176.927 56	17.149	17.634	558354405855	6_8	14	
OGLE-LMC-ACEP-037	5:19:16.67	−70:11:58.4	F	1.257 74	52 156.5207	17.132	17.743	558361296449	5_5	15	a
OGLE-LMC-ACEP-036	5:18:58.85	−69:26:47.8	F	1.257 982	504 55.673 96	17.160	17.787	558355324744	6_4	23	
OGLE-LMC-ACEP-052	5:31:01.53	−70:42:22.2	F	1.262 555	52 167.0715	17.008	17.577	558361664456	5_5	15	
OGLE-LMC-ACEP-046	5:26:27.17	−69:58:57.0	F	1.263 717	50 454.399 55	17.264	17.851	558356990050	6_5	9	
OGLE-LMC-ACEP-021	5:06:37.49	−68:23:40.3	F	1.295 843	50 725.625 18	17.188	17.827	558351789022	7_3	16	
OGLE-LMC-ACEP-044	5:25:54.11	−69:26:52.9	F	1.308 509	50 455.106 39	17.052	17.609	558356474792	6_5	9	
OGLE-LMC-ACEP-032	5:15:56.13	−69:01:29.1	F	1.316 022	50 456.811 67	17.167	17.780	558355007611	6_4	14	
OGLE-LMC-ACEP-065	5:40:03.04	−70:04:47.8	F	1.321 5432	50 725.780 28	17.041	17.508	558358103119	6_6	0	b
OGLE-LMC-ACEP-016	5:01:36.69	−67:51:33.1	F	1.545 67	52 166.4502	16.926	17.448	558351480147	7_3	16	
OGLE-LMC-ACEP-048	5:27:12.12	−69:37:19.6	F	1.545 893	50 454.481 93	16.718	17.324	558356636279	6_5	9	
OGLE-LMC-ACEP-055	5:31:41.11	−68:44:37.7	F	1.606 665	52 189.7241	17.011	17.603	558357237330	6_6	14	
OGLE-LMC-ACEP-057	5:31:49.88	−70:46:30.0	F	1.710 008	52 167.362 19	16.813	17.455	558361710363	5_5	15	
OGLE-LMC-ACEP-026	5:10:42.62	−68:48:19.6	F	1.738 745	50 457.225 81	16.816	17.483	558354874727	6_4	14	
OGLE-LMC-ACEP-053	5:31:06.20	−68:43:45.3	F	1.888 099	52 166.630 19	16.738	17.299	558355958053	6_5	23	a
OGLE-LMC-ACEP-047	5:27:05.27	−71:23:33.4	F	2.177 985	52 166.330 26	16.881	17.482	558362082677	5_5	15	
OGLE-LMC-ACEP-014	5:00:08.26	−67:54:04.3	F	2.291 346	52 164.638 44	16.639	17.241	558351518318	7_3	16	

[a] Stars showing significant blending but with useful light curves (see Figs 2–4).
[b] Stars without K_s VMC data (see Fig. 2).
[c] Stars showing significant blending and having unusable light curves (see Figs 2 and 5).

typically ranges from 0.2 to 0.5 mag, the average correction over the 42 ACs considered here, is as small as -3.0 ± 1.0 mmag and can be safely neglected. In conclusion, for ACs, as well as for CCs (see Ripepi et al. 2012b), to a very good approximation, the VISTA and 2MASS K_s can be considered equivalent.

3 OPTICAL PERIOD–LUMINOSITY, PERIOD–LUMINOSITY–COLOUR AND PERIOD–WESENHEIT RELATIONS

Before presenting the results in the NIR bands, in this section, we derive the coefficients of the optical (V, I) *P–L*, *P–L–C* and

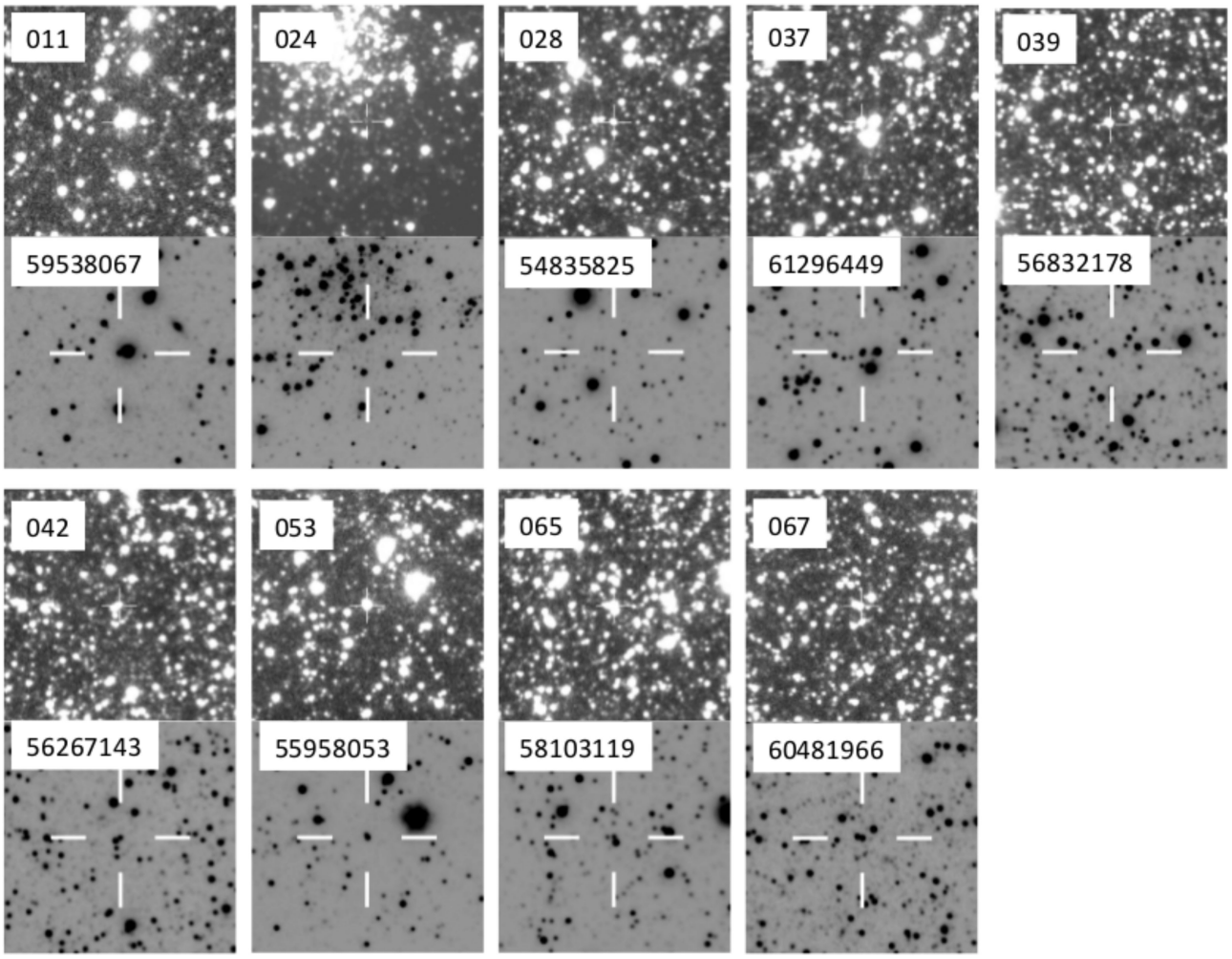

Figure 2. Sky pictures for nine problematic stars extracted from the VMC (lower panels) and the OGLE III (upper panels) archives. The target is identified in the single-epoch VMC images by a label showing the last eight digits of the VMC identification. Similarly the corresponding OGLE III identification is reported with three digits (i.e. without the prefix 'OGLE-LMC-AC-').

Table 3. K_s time series photometry of the ACs.

HJD-240 0000	K_s	σ_{K_s}
AC OGLE-LMC-ACEP-007		
562 67.810 39	17.118	0.039
563 16.644 76	16.921	0.032
563 18.553 54	16.899	0.030
563 22.632 75	17.170	0.036
563 28.570 27	16.925	0.030
563 34.543 72	16.933	0.036
563 41.531 32	17.200	0.042
563 47.560 46	17.036	0.032
563 71.532 52	16.923	0.034
563 72.519 81	16.952	0.034
563 75.522 38	17.112	0.034

Note. Table 3 is published in its entirety only in the electronic edition of the journal. A portion is shown here for guidance regarding its form and content.

Wesenheit-$W(V, I)$ relations, based on the OGLE data, since they are still lacking in the literature. Indeed, neither Soszyński et al. (2008) nor Fiorentino & Monelli (2012) published these relations, although they showed them in some figures. In this case, we have used the whole sample of ACs detected in the LMC by the OGLE III/IV surveys.

The first step is to correct for reddening, which unfortunately is rather variable in the LMC and hence needs to be evaluated locally. To this aim, we adopted the recent estimates by Haschke, Grebel & Duffau (2011). Individual $E(V - I)$ reddening values for the 42 ACs with useful VMC data are reported in column 7 of Table 4. In Section 5, we will check the soundness of these reddening values.

The second step consists of accounting for the inclination of the LMC disc-like structure by deprojecting each AC with respect to the LMC centre. We followed the procedure outlined in van der Marel & Cioni (2001) and adopted their values of the LMC centre, inclination and position angle of the line of nodes (see column 8 of Table 4).

Finally, we performed least-squares fits to the data of F- and FO-mode variables separately, adopting equations of the form $\mathrm{Mag} = \alpha + \beta \log P$, with Mag $= V, I$. The best-fitting relationships are shown in the left-hand panels of Fig. 6, their coefficients are provided in the first portion of Table 5. We note that in all panels of this figure, the stars plotted with crosses and open circles were rejected from the fit because they are 2.5–3σ off the regression line. In particular, the three objects with the longest periods, namely OGLE-LMC-ACEP-014, 033 and 047 (crosses in Fig. 6) are likely

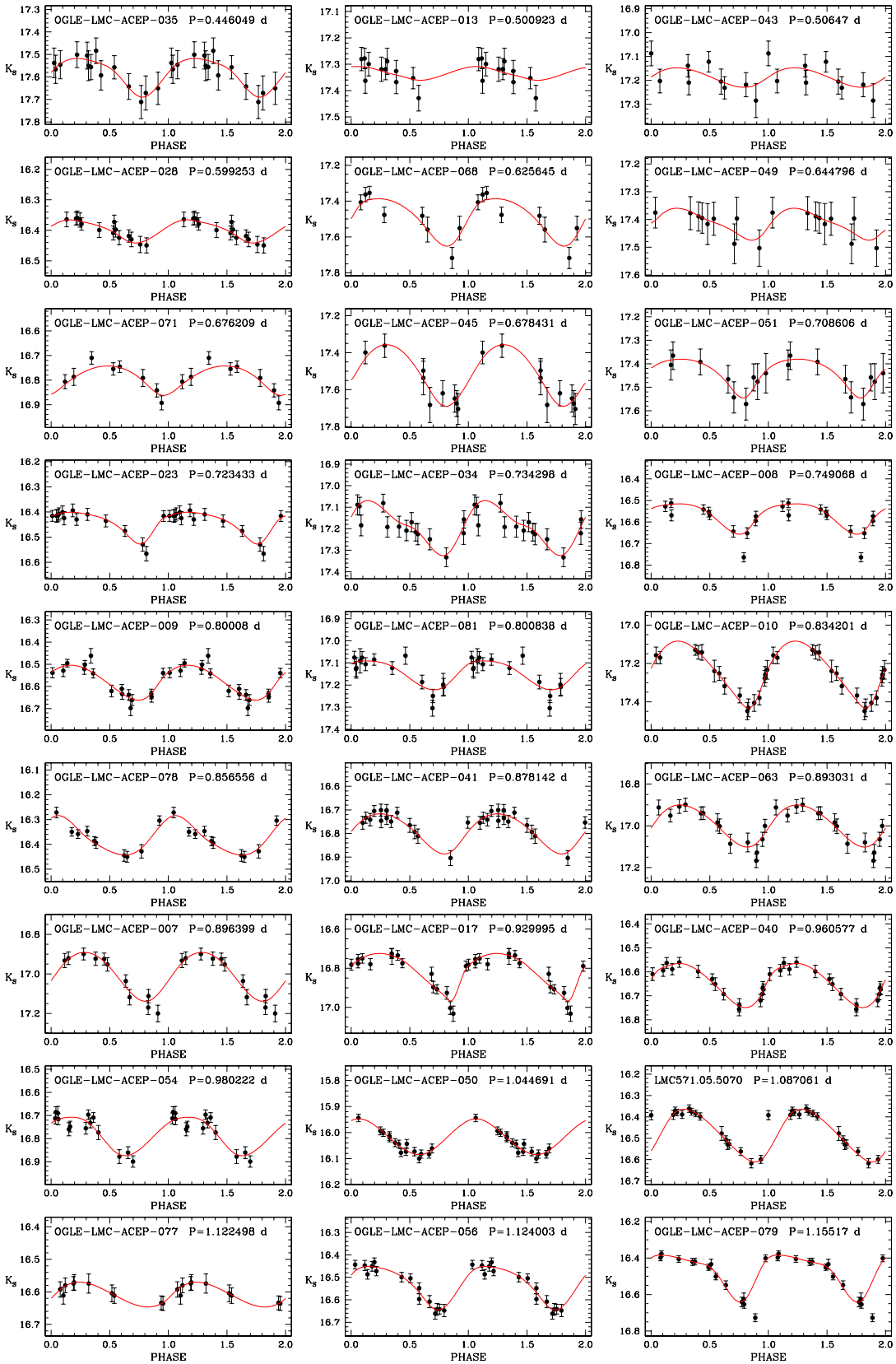

Figure 3. K_s-band light curves for 27 of the 42 ACs with usable data discussed in this paper. Stars are displayed in order of increasing period. Solid lines represent spline best fits to the data (see text). In each panel, we report OGLE's identification number and period.

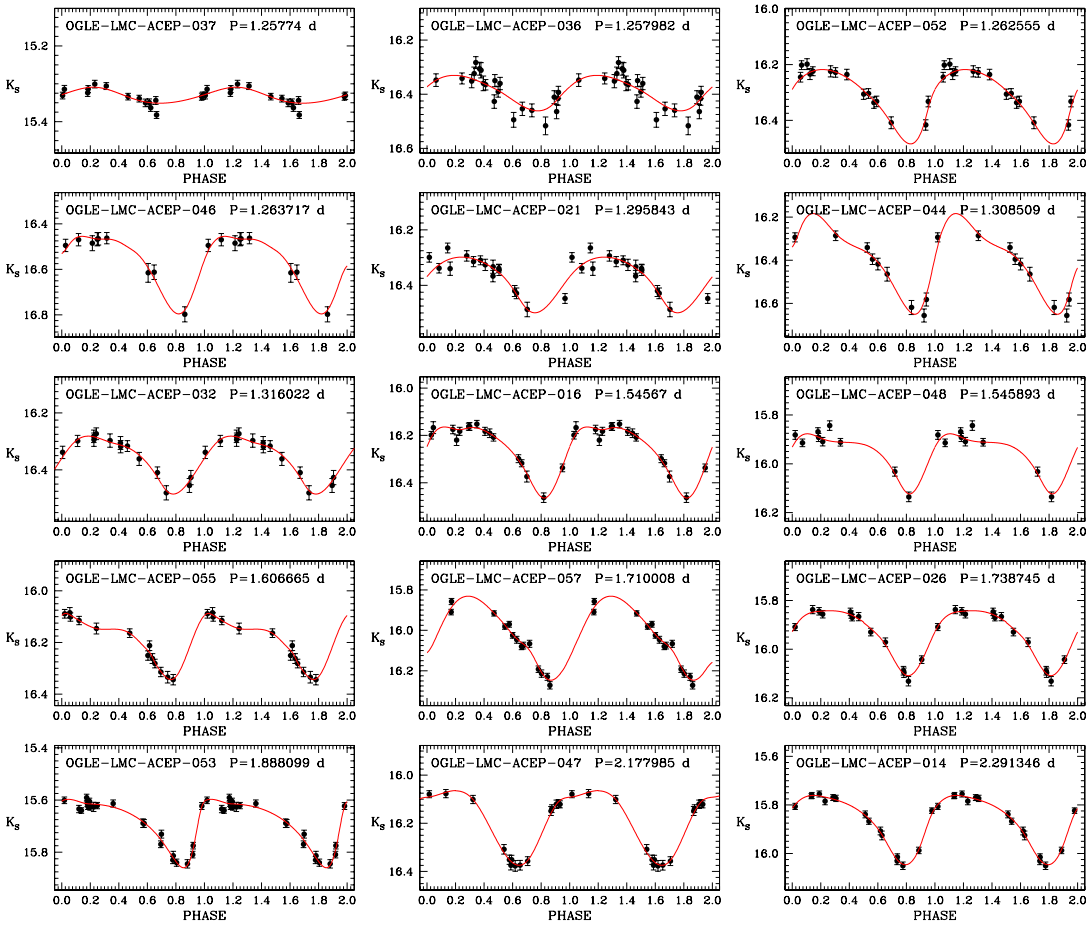

Figure 4. As in Fig. 3 but for the remaining 15 ACs of our sample.

not ACs but rather members of some different variable classes such as BL Herculis stars. Indeed, looking at fig. 1 in Soszyński et al. (2008), it is clear that some confusion can be possible between ACs and BL Her pulsators at the periods of interest. Additional stars that were not used in at least one of the regressions are OGLE-LMC-ACEP-022, 024, 028, 042, 059 and 083. All these objects, with the possible exception of 022, show some observational problems. In particular, the stars 024, 042 and 028 will be discussed in detail in the next section, since they are problematic also in the VMC data (see Fig. 2). As for the remaining three, we inspected the OGLE images and light curves, finding that in the case of the star 083 there is a strong background variation close to the object (possibly close to an edge of the CCD) and the star light curves appear to be rather noisy. Stars 022 and 059 are surrounded by a number of close companions and both of them show a rather noisy light curve, especially star 059, that has also a large $(V - I)$ colour (>1.2 mag).

In addition to the V, I P–L relations, we can also derive the P–W and P–L–C relations. The advantages of using these relations instead of a simple P–L relation have been widely discussed in the literature (see e.g. Marconi et al. 2004, in the case of ACs). Briefly, these relations include a colour term with a coefficient that, in the case of the P–L–C relation, takes into account the colour distribution of the variable stars within the instability strip, whereas in the case of the Wesenheit function corresponds to the ratio between total-to-selective extinction in the filter pair (Madore 1982; Caputo, Marconi & Musella 2000), thus making the Wesenheit relations reddening free by definition. We expect these relations to have much smaller dispersion than a simple P–L relation, even if the scatter reduction for ACs is not as significant as in the case of CCs (see e.g. Marconi, Fiorentino & Caputo 2004; Marconi, Musella & Fiorentino 2005). In fact, for CCs, a strict mass–luminosity ($M-L$) relation is predicted to exist by stellar evolution computations for He burning intermediate-mass stars, which makes the P–L–C relation hold for each individual pulsator (see e.g. Caputo et al. 2000, for details). Unfortunately, the ACs are not characterized by such a strict ML relation, thus the resulting P–L–C and P–W relations include the possible effect of mass differences at fixed luminosity level.

The P–W and P–L–C relations are usually calculated using the $(V - I)$ colour. The coefficients of the relations derived with this procedure for the LMC ACs are provided in the lower portions of Table 5. The relations are shown in the right-hand panels of Fig. 6. The dispersion of the P–W and P–L–C relations is of the order of ~ 0.15 mag (see Table 5), hence smaller than that for the P–L relation but larger than in the case of CCs (see e.g. Soszyński et al. 2008, who found a $\sigma = 0.08$ mag for the P–$W(V, I)$ relation).

4 K_s-BAND PERIOD–LUMINOSITY AND PERIOD–WESENHEIT RELATIONS

By analogy to the optical V, I bands, we can calculate the P–L and P–W relationships in the K_s band. Our sample consist of 32 F-mode and 10 FO-mode ACs that are sufficient to provide statistically meaningful P–L and P–W relations. For both modes of pulsation, our sample maps the whole range of periods covered by the LMC ACs, as shown in Fig. 6, where we have plotted in green and magenta colours the F- and FO-mode objects observed by VMC, respectively.

Table 4. Results for the 42 ACs with useful light curves analysed in this paper. The columns report: (1) OGLE identification, (2) mode of pulsation, (3) period, (4) intensity-averaged K_s magnitude, (5) uncertainty on the $\langle K_s \rangle$, (6) peak-to-peak amplitude in K_s, (7) adopted reddening and (8) correction in magnitude due to the deprojection.

ID	M	Period (d)	$\langle K_s \rangle$ (mag)	$\sigma_{\langle K_s \rangle}$ (mag)	Amp(K_s) (mag)	$E(V-I)$ (mag)	Δ (mag)
(1)	(2)	(3)	(4)	(5)	(6)	(7)	(8)
OGLE-LMC-ACEP-035	FO	0.446 049	17.585	0.026	0.17	0.07	0.026
OGLE-LMC-ACEP-013	FO	0.500 923	17.334	0.033	0.06	0.03	0.068
OGLE-LMC-ACEP-043	FO	0.506 47	17.186	0.051	0.08	0.09	0.013
OGLE-LMC-ACEP-028	FO	0.599 253	16.399	0.010	0.08	0.06	0.040
OGLE-LMC-ACEP-068	F	0.625 645	17.490	0.049	0.26	0.06	−0.042
OGLE-LMC-ACEP-049	F	0.644 796	17.412	0.028	0.12	0.04	0.003
OGLE-LMC-ACEP-071	FO	0.676 209	16.790	0.015	0.12	0.07	−0.053
OGLE-LMC-ACEP-045	F	0.678 431	17.499	0.045	0.33	0.11	0.008
OGLE-LMC-ACEP-051	F	0.708 606	17.437	0.023	0.17	0.10	0.000
OGLE-LMC-ACEP-023	FO	0.723 433	16.444	0.005	0.13	0.08	0.052
OGLE-LMC-ACEP-034	F	0.734 298	17.186	0.022	0.26	0.13	0.028
OGLE-LMC-ACEP-008	FO	0.749 068	16.567	0.007	0.14	0.08	0.072
OGLE-LMC-ACEP-009	FO	0.800 08	16.575	0.014	0.16	0.06	0.081
OGLE-LMC-ACEP-081	F	0.800 838	17.147	0.017	0.13	0.07	−0.090
OGLE-LMC-ACEP-010	F	0.834 201	17.225	0.015	0.35	0.11	0.077
OGLE-LMC-ACEP-078	FO	0.856 556	16.372	0.018	0.16	0.09	−0.057
OGLE-LMC-ACEP-041	F	0.878 142	16.790	0.020	0.17	0.09	0.021
OGLE-LMC-ACEP-063	F	0.893 031	16.990	0.026	0.20	0.18	−0.020
OGLE-LMC-ACEP-007	F	0.896 399	17.002	0.020	0.25	0.06	0.073
OGLE-LMC-ACEP-017	F	0.929 995	16.810	0.015	0.25	0.06	0.070
OGLE-LMC-ACEP-040	F	0.960 577	16.644	0.012	0.18	0.09	0.021
OGLE-LMC-ACEP-054	F	0.980 222	16.781	0.029	0.17	0.26	−0.000
OGLE-LMC-ACEP-050	FO	1.044 691	16.016	0.011	0.14	0.07	0.003
LMC571.05.5070	F	1.087 061	16.479	0.007	0.25	0.08	−0.072
OGLE-LMC-ACEP-077	F	1.122 498	16.608	0.002	0.08	0.07	−0.062
OGLE-LMC-ACEP-056	F	1.124 003	16.527	0.019	0.19	0.06	−0.002
OGLE-LMC-ACEP-079	F	1.155 17	16.471	0.013	0.26	0.05	−0.085
OGLE-LMC-ACEP-037	F	1.257 74	15.332	0.007	0.04	0.08	0.024
OGLE-LMC-ACEP-036	F	1.257 982	16.388	0.022	0.13	0.08	0.023
OGLE-LMC-ACEP-052	F	1.262 555	16.316	0.011	0.27	0.07	0.001
OGLE-LMC-ACEP-046	F	1.263 717	16.570	0.016	0.35	0.03	0.008
OGLE-LMC-ACEP-021	F	1.295 843	16.377	0.027	0.20	0.07	0.058
OGLE-LMC-ACEP-044	F	1.308 509	16.380	0.024	0.48	0.06	0.007
OGLE-LMC-ACEP-032	F	1.316 022	16.360	0.010	0.20	0.06	0.032
OGLE-LMC-ACEP-016	F	1.545 67	16.261	0.006	0.30	0.05	0.073
OGLE-LMC-ACEP-048	F	1.545 893	15.958	0.018	0.25	0.07	0.005
OGLE-LMC-ACEP-055	F	1.606 665	16.188	0.010	0.26	0.08	−0.003
OGLE-LMC-ACEP-057	F	1.710 008	16.006	0.017	0.43	0.07	−0.001
OGLE-LMC-ACEP-026	F	1.738 745	15.932	0.011	0.27	0.08	0.046
OGLE-LMC-ACEP-053	F	1.888 099	15.682	0.011	0.26	0.11	−0.002
OGLE-LMC-ACEP-047	F	2.177 985	16.181	0.009	0.31	0.07	0.012
OGLE-LMC-ACEP-014	F	2.291 346	15.862	0.008	0.29	0.04	0.076

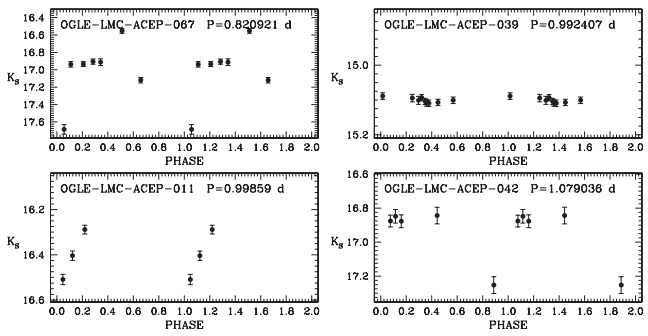

Figure 5. Light curves for four problematic stars (see text).

The K_s-band P–L and P–W relations obtained are displayed in Fig. 7, whereas their coefficients are summarized in Table 6. Three F-mode and one FO-mode stars were excluded from the fit because they are more than 2σ off the regression lines. The stars OGLE-LMC-ACEP-037 and 028, an F- and an FO-mode pulsator, respectively, are shown with empty circles in Fig. 7. They have rather 'normal' light curves, but at least the star 037 is clearly blended (see Fig. 2). The star 028 also exhibit an unusual colour (see Section 5 and Fig. 9) and we hypothesize that it may be blended; however, we do not have enough resolution to detect the contaminant star. The two additional F-mode ACs excluded from the fit (namely OGLE-LMC-ACEP-014 and OGLE-LMC-ACEP-047, shown as crosses in Fig. 7) are the stars with the longest periods. They were excluded also in the optical analysis as we suspect they could possibly belong to a

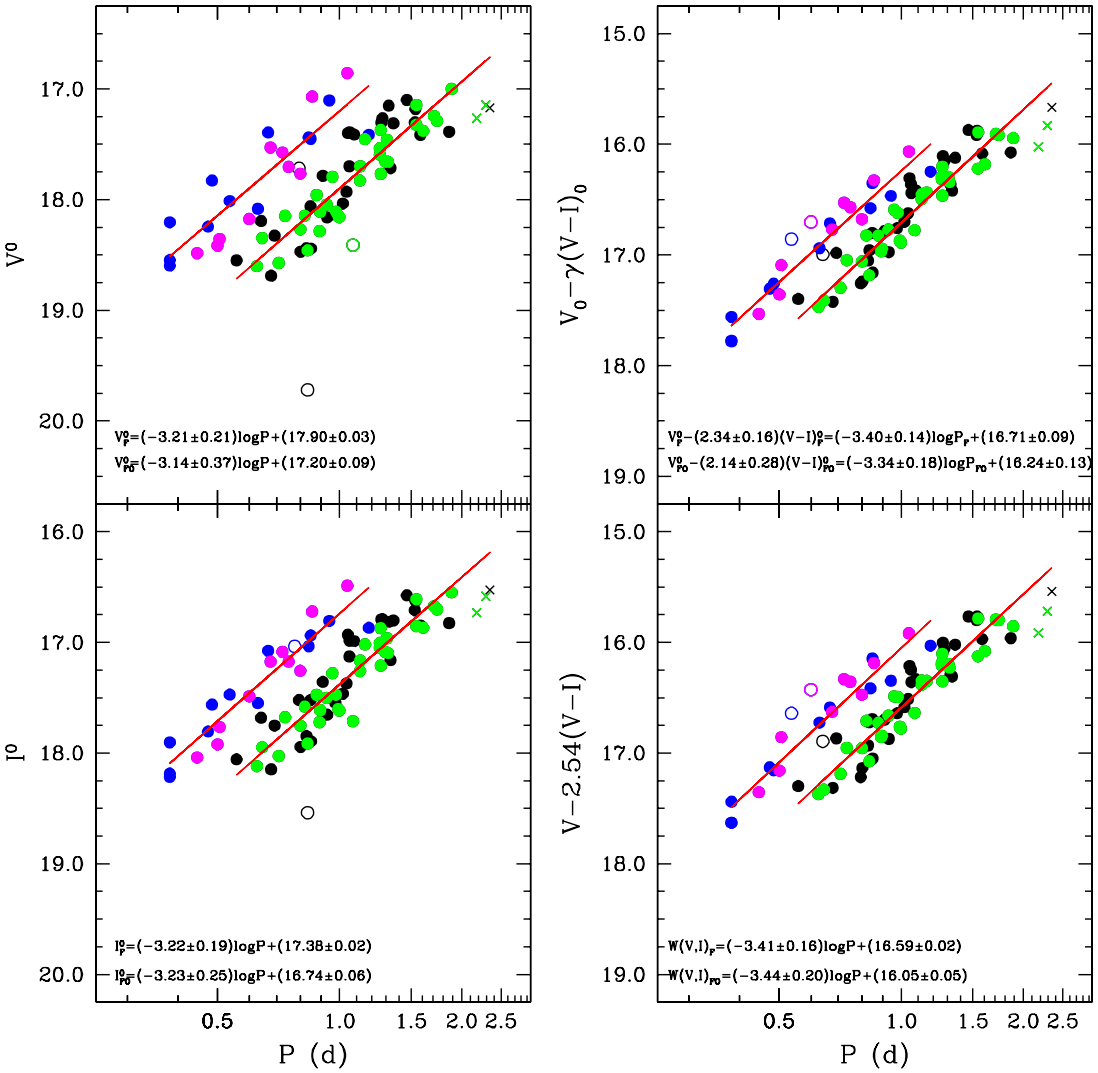

Figure 6. Optical *P–L*, *P–W* and *P–L–C* relations for F and FO ACs. The Wesenheit function is defined as: $W(V, I) = V - 2.54\,(V - I)$. In each panel, green and black filled circles are OGLE F pulsators, blue and magenta filled circles are OGLE FO pulsators, with (in green and magenta) or without (in black and blue) VMC K_s measurements. Empty circles and crosses mark pulsators that were discarded in the derivation of the *P–L* and *P–W* (and the optical *P–L–C*) relations. In particular, the three stars with longest periods (crosses) likely are not ACs and rather belong to a different type of variability. In all panels, the red lines show the best fits to the data, with the corresponding relationships labelled at the bottom.

Table 5. Optical *P–L*, *P–W* and *P–L–C* relations for F and FO ACs. The Wesenheit function is defined as: $W(V, I) = V - 2.54\,(V - I)$.

Mode	α	σ_α	β	σ_β	γ	σ_γ	rms
			$V^0 = \alpha + \beta \log P$				
F	17.90	0.03	−3.21	0.21			0.20
FO	17.20	0.09	−3.14	0.37			0.23
			$I^0 = \alpha + \beta \log P$				
F	17.38	0.02	−3.22	0.19			0.18
FO	16.74	0.06	−3.23	0.25			0.16
			$W(V, I) = \alpha + \beta \log P$				
F	16.59	0.02	−3.41	0.16			0.15
FO	16.05	0.05	−3.44	0.22			0.13
			$V^0 = \alpha + \beta \log P + \gamma (V - I)^0$				
F	16.71	0.09	−3.40	0.14	2.34	0.16	0.14
FO	16.24	0.13	−3.34	0.18	2.14	0.28	0.12

separate class of variables. We note that, as for CCs, moving to the NIR the dispersion of the AC *P–L* and $W(V, K_s)$ relations decreases. We also made an attempt to calculate *P–L–C* relations in the form $K_s^0 = f(\log P, (V - K_s)_0)$, but the colour term coefficient turned out to be statistically equal to zero. This is not very surprising given the relatively small number of pulsators and the almost identical dispersions of the *P–L* and *P–W* relations. Hence, according to this data set, in the NIR filters it seems that there is no great advantage in using the AC *P–L–C* or pseudo *P–L–C* relations instead of the *P–L*.

5 COMPARISON WITH LITERATURE AND APPLICATION TO REAL CASES

To compare our *P–L*s for ACs with the relations available in the literature, we first need to set the absolute zero-points. This can be done by assuming a proper value for the distance to the host galaxy, the LMC. We have adopted our own evaluation based on

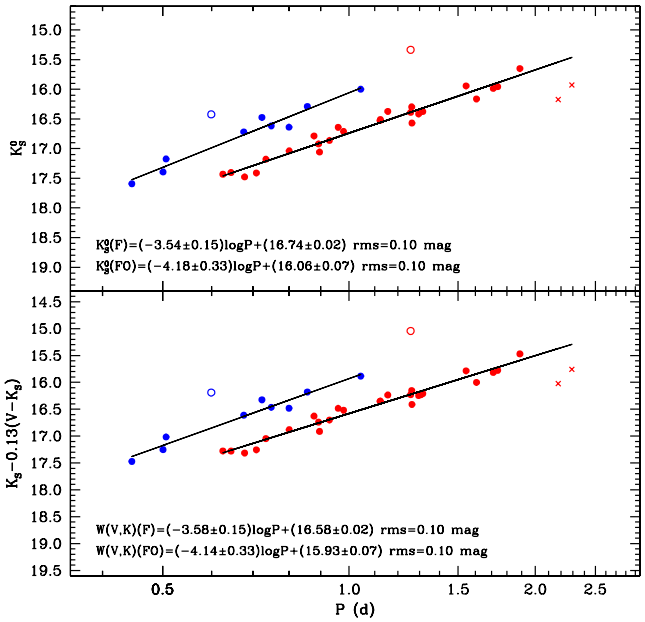

Figure 7. Top panel: K_s-band *P–L* relation for F- and FO-mode ACs (red and blue symbols, respectively). Filled circles show the objects used for the least-squares fits. Stars marked by open circles and crosses were discarded (see text for detail). The solid line is the least-squares fit to the data. Bottom panel: as for the top panel but for the Wesenheit function, which is defined as labelled in the figure.

Table 6. NIR *P–L* and *P–W* relations for F- and FO-mode ACs. The Wesenheit function is defined as: $W(V, K) = K_s - 0.13\,(V - K_s)$. Note that all the results are in the VISTA photometric system.

Mode	α	σ_α	β	σ_β	γ	σ_γ	rms
			$K_s^0 = \alpha + \beta \log P$				
F	16.74	0.02	−3.54	0.15			0.10
FO	16.06	0.07	−4.18	0.33			0.10
			$W(V, K_s) = \alpha + \beta \log P$				
F	16.58	0.02	−3.58	0.15			0.10
F	15.93	0.07	−4.14	0.33			0.10

the absolute calibrations of the *P–L*, *P–L–C* and $W(V, K_s)$ relations for CCs in the LMC presented in Ripepi et al. (2012b). In that paper, we used the trigonometric parallaxes of Galactic Cepheids as well as Baade–Wesselink measurements of Cepheids in the LMC to evaluate $DM^0_{LMC} = 18.46 \pm 0.03$ mag (see Ripepi et al. 2012b, for full details). This distance modulus is in very good agreement with current literature estimates for the distance to the LMC as nicely reviewed by Walker (2012) and with the very recent and precise value by Pietrzyński et al. (2013) based on eclipsing binaries. Results of this comparison in the optical are summarized in the first part of Table 7 and graphically shown in Fig. 8 for the *P–L* and the Wesenheit relations, respectively.

The upper panel of Fig. 8 shows the comparison of our *P–L*s with the relations derived empirically by Pritzl et al. (2002) and Marconi et al. (2004) on the basis of a few tens of ACs belonging to a number of dwarf spheroidal galaxies (dSph) orbiting the Milky Way and M31 spirals. There is a clear disagreement between our results and the literature. This is likely due to a number of reasons: (i) the very different coverage of the AC instability strip, which is much more uniformly and completely covered in the LMC sample; (ii) at shorter periods ($P \sim 0.4$-0.5 d), it is easy to confuse F- and FO-mode pulsators, especially in the dSphs where samples are generally rather small; (iii) the non-homogeneous dSph sample. Better agreement, at least for the F-mode pulsators, can be seen in the bottom panel of Fig. 8, where we compare our $W(V, I)$ function with those by Marconi et al. (2004), the only published relation to date. The better agreement in this case is probably due to the much lower dependence of the $W(V, I)$ with respect to the *P–L* on the way the pulsators populate the instability strip.

Marconi et al. (2004) also published mass-dependent, *P–L–C* and Wesenheit (the latter only for F-mode pulsators) relations for ACs calculated on the basis of non-linear, non-local time-dependent convective pulsation models. The lower portion of Table 7 reports the comparison between Marconi et al. (2004) theoretical models and our results. There is good agreement for the slope of the P–$W(V, I)$ relations; however, our zero-point implies a stellar mass of $M \sim 1.3\,M_\odot$, at the lower end of the allowed range for ACs.

As for the *P–L–C*, both the slopes and the zero-point disagree by more than 1σ. We do not have a clear explanation for these discrepancies; however, if the reddening values we have adopted for the ACs are correct, the disagreement could in principle be related to uncertainties in the theoretical colour–temperature relations.

There are no other empirical NIR relations in the literature we are aware of; hence, we can compare our results only with the colour–colour and the P–$W(V, K_s)$ relations derived by Marconi et al. (2004) from the theory of stellar pulsation. The top panel of Fig. 9 shows this comparison for the 42 pulsators analysed in this paper in the $(V - I)_0$–$(V - K_s)_0$ plane. Overall, the agreement is very satisfactory. The residual discrepancy can be minimized by a difference in the adopted reddening of only $\langle \Delta E(V - I) \rangle = -0.01 \pm 0.02$ mag. This is a confirmation that the reddening values adopted in this paper are well established. An inspection of the figure confirms that the two stars OGLE-LMC-ACEP-037 and 028 (empty circles), previously excluded from the *P–L* and *P–W* derivation, are highly deviant also in the colour–colour plane. In addition, we find a third discrepant star in this plane: OGLE-LMC-ACEP-053 (empty star). Also, this object is clearly blended (see Fig. 2) so that its strange position in the colour–colour plane can be easily explained. Since this AC shows a rather normal light curve and it is not deviant e.g. in the *P–L* relation, we conclude that its photometry is only mildly affected by the blending star.

The lower panel of Fig. 9 shows the comparison between our F-mode P–$W(V, K_s)$ relation and theoretical predictions (not available for FO-mode pulsators), for three different choices of the AC mass encompassing approximately the whole range of allowed values for this parameter, namely $M = 1.3$, 1.6 and $1.9\,M_\odot$. There is good agreement for the slope of the P–$W(V, K_s)$ relations, whereas, as already found for the optical P–$W(V, I)$, our zero-point seems to favour the smallest value of $M = 1.3\,M_\odot$, for the mass.

5.1 Application of the optical *P–W* relation

In the previous sections, we have shown that the $P-W(V, I)$ relation is likely the best tool we have to use the ACs as standard candles. Indeed, the $P-W(V, I)$ relation does not depend on the reddening and on how the pulsators populate the instability strip. This obviously holds also for the $P - W(V, K_s)$. However, at present, the lack of NIR observations of ACs in other galaxies limits severely the use of this relation. On the contrary, V, I data are available for a significant number of ACs belonging to a few dwarf galaxies in the Local

Table 7. Literature values for the coefficients of the *P–L*, *P–W* and *P–L–C* relations, for F and FO ACs. The Wesenheit functions are defined as: $W(V, I) = V - 2.54(V - I)$ and $W(V, K_s) = K_s - 0.13(V - K_s)$. In the K_s, the photometry of previous studies was converted to the 2MASS system, for consistency with our results (see Section 2).

Mode	α	σ_α	β	σ_β	γ	σ_γ	rms	Source
			$M_V^0 = \alpha + \beta \log P$					
F	−0.56	0.04	−3.21	0.21			0.20	This paper
F	−0.71	0.03	−2.64	0.17				Pritzl et al. (2002)
F	−0.70	0.14	−2.73				0.14	Marconi et al. (2004)[a]
FO	−1.26	0.09	−3.14	0.37			0.23	This paper
FO	−1.61	0.07	−3.74	0.20			0.25	Pritzl et al. (2002)
FO	−1.58	0.25	−2.95				0.25	Marconi et al. (2004)[a]
			$W(V, I) = \alpha + \beta \log P$					
F	−1.87	0.04	−3.41	0.16			0.15	This paper
F	−1.93	0.20	−3.34				0.20	Marconi et al. (2004)[a]
F	$-1.74-1.83 \log M$	0.20	−3.34				0.20	Marconi et al. (2004)[b]
FO	−2.41	0.06	−3.44	0.22			0.13	This paper
FO	−2.52	0.20	−2.51				0.20	Marconi et al. (2004)[a]
			$M_V^0 = \alpha + \beta \log P + \gamma(V - I)_0$					
F	−1.75	0.09	−3.40	0.14	2.34	0.16	0.14	This paper
F	$-1.83-1.89 \log M$		−2.93		2.73		0.01	Marconi et al. (2004)[b]
FO	−2.22	0.13	−3.34	0.18	2.14	0.28	0.12	This paper
FO	$-2.24-1.73 \log M$		−3.09		2.67		0.01	Marconi et al. (2004)[b]
			$K_s = \alpha + \beta \log P$					
F	−1.72	0.04	−3.54	0.15			0.10	This paper
FO	−2.40	0.07	−4.18	0.33			0.10	This paper
			$W(V, K_s) = \alpha + \beta \log P$					
F	−1.88	0.04	−3.58	0.15			0.10	This paper
F	$-1.71 - 1.83 \log M$		−2.93				0.04	Marconi et al. (2004)[b, c]
FO	−2.53	0.07	−4.14	0.33			0.10	This paper

[a]Empirical.
[b]Theoretical, the value of the mass ranges from 1.3 to 1.9 $M_\odot$.
[c]Models transformed to the Johnson system: for ACs K(Johnson) ≈ K(SAAO) (see Bessell & Brett 1988). K_s(2MASS) = K(SAAO) + 0.02$(J - K)$(SAAO)−0.025 (Carpenter 2001).

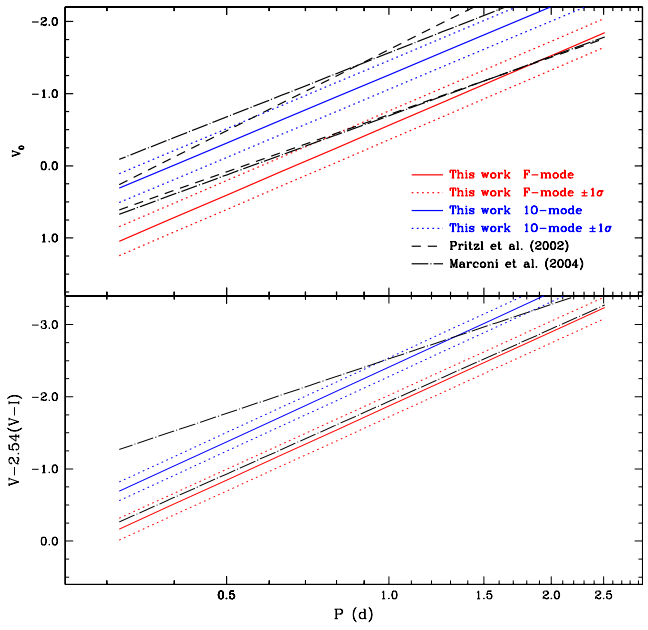

Figure 8. Comparison between the optical *P–L* (top panel) and *P–W*(*V*, *I*) relations (bottom panel) for F- and FO-mode ACs derived in this paper with the literature results.

Group that can be used to verify the ability of our $P-W(V, I)$ to estimate the distance to the host systems by comparing AC-based and RR-Lyrae-based distance determinations.

To our knowledge, there are only three dwarf galaxies with a significant number of ACs measured in the V, I bands, namely Fornax (Bersier & Wood 2002), Leo T (Clementini et al. 2012) and Phoenix (Gallart et al. 2004). There is no clear separation between F- and FO-mode pulsators in these galaxies (see Pritzl et al. 2002; Marconi et al. 2004); hence, we used our own *P–W* relation to perform a tentative subdivision of the samples into the two modes. The result of the overall procedure is shown in Fig. 10, where the different panels report the results for the three aforementioned galaxies. The distance moduli labelled in the figures were obtained to adjust simultaneously F-mode and FO-mode pulsators, and weighting the results to take into account the number of pulsators in each of the two modes. Errors on the derived distances are dominated by the dispersion of the LMC $P - W(V, I)$, whereas the uncertainty of the LMC distance is significantly smaller.

In Table 8, we compare the distances obtained from the ACs and literature values based on RR Lyrae or other distance indicators. Our distance modulus for the Fornax dSph is systematically smaller than all the other determinations, but still in agreement with most of them within 1σ. In contrast, the agreement is rather good for Leo T and excellent for Phoenix. On this basis, it is not easy to explain why we find such shorter distances for Fornax dSph. New observations,

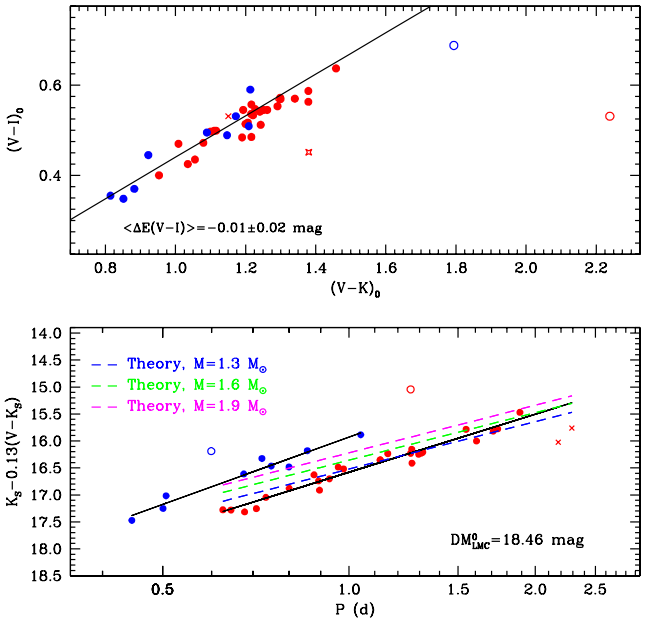

Figure 9. Top panel: $(V - I)_0$ versus $(V - K_s)_0$ plot for the F-mode ACs analysed in this paper. Symbols are as in Fig. 7. The solid line represents the theoretical relation by Marconi et al. (2004). The theoretical $(V - K_s)_0$ was converted to the 2MASS system using the relations in Table 7. Bottom panel: comparison between the observed Wesenheit K_s-band relation for F-mode (solid line; note that the FO-mode relation is shown, too) and the predictions by Marconi et al. (2004) for three different choices of the pulsator mass (dashed lines, see labels).

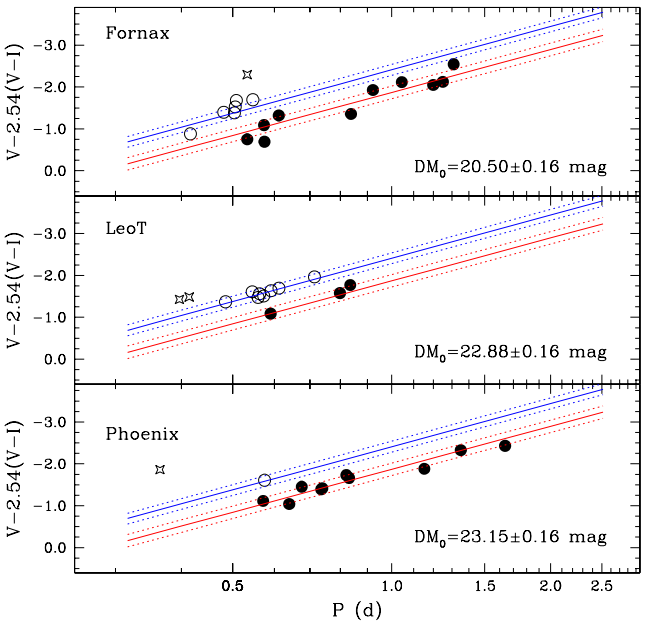

Figure 10. Optical $P-W(V, I)$ relations for ACs in a number of Local Group dwarf galaxies in comparison with the results obtained in this paper. F- and FO-mode ACs are marked by filled and empty circles, respectively; starred symbols refer to objects with uncertain classification that were not used in calculating the distances. Red and blue lines show this work $P-W(V, I)$ for F- and FO-mode ACs, respectively. True distance moduli estimated from these relations are labelled.

Table 8. Comparison between distances derived from the ACs in this paper and the literature values for the Fornax, Leo T and Phoenix Local Group dwarf.

Method	DM_0	Reference
Fornax: DM_0(ACs) = 20.50 ± 0.16 mag (15 ACs)		
TRGB	20.76 ± 0.20	(1)
Red Clump	20.66	(2)
TRGB	20.65 ± 0.11	(2)
Red Clump	20.86 ± 0.01	(3)
RR Lyrae	20.72 ± 0.10	(4)
TRGB	20.75 ± 0.19	(5)
HB	20.70 ± 0.12	(6)
TRGB	20.84 ± 0.18	(7)
RR Lyrae	20.66 ± 0.07	(8)
Leo T: DM_0(ACs) = 22.88 ± 0.16 mag (11 ACs)		
TRGB	23.1 ± 0.2	(9)
SFH-Fitting	23.05	(10)
RR Lyrae	23.06 ± 0.15	(11)
Phoenix: DM_0(ACs) = 23.15 ± 0.16 mag (11 ACs)		
TRGB	23.0 ± 0.1	(12)
TRGB	23.21 ± 0.08	(13)
TRGB	23.11	(14)
Mira	23.10 ± 0.18	(15)
TRGB	23.09 ± 0.10	(16)

References: (1) Buonanno et al. (1999); (2) Bersier (2000); (3) Pietrzyński, Gieren & Udalski (2003); (4) Greco et al. (2005); (5) Gullieuszik et al. (2007); (6) Rizzi et al. (2006); (7) Pietrzyński et al. (2009); (8) Greco et al. (2009); (9) Irwin et al. (2007); (10) Weisz et al. (2012); (11) Clementini et al. (2012); (12) Martínez-Delgado, Gallart & Aparicio (1999); (13) Held, Saviane & Momany (1999); (14) Holtzman, Smith & Grillmair (2000); (15) Menzies et al. (2008); (16) Hidalgo et al. (2009).

including the complete sample of ACs belonging to this very large galaxy are needed to clarify this point.

Concluding, the $P - W(V, I)$ derived in this paper is a reliable tool for the determination of the distance to galaxies hosting significant samples of ACs.

6 SUMMARY AND CONCLUSIONS

We have presented the first light curves in the NIR K_s band for ACs. In particular, our sample consists of 46 AC pulsators (36 F-mode and 10 FO-mode) located in the LMC and observed by the VMC survey. Our light curves are well sampled with the number of epochs ranging from 8 to 23. In spite of the faintness of the LMC ACs, these data allowed us to obtain very precise mean K_s magnitudes for the pulsators, with average errors of the order of 0.01 mag.

The $\langle K_s \rangle$ magnitudes were used to build the first *P–L* and *P–W* relations in the NIR for F- and FO-mode ACs. At the same time, we exploited the OGLE optical (V, I) data for ACs to construct accurate optical *P–L*, *P–L–C* and *P–W* relations both for F- and FO-mode ACs. These relations were obtained for the first time from a sample of pulsators covering in a uniform and complete way the AC instability strip.

The application of the P–$W(V, I)$ relation to three dwarf galaxies hosting significant populations of ACs, revealed that this relation

is a valuable tool for deriving distances within the Local Group. Due to the lower dispersion, we expect that the P–$W(V, K_s)$ first derived in this paper will become an even better tool for measuring distances to galaxies hosting ACs. More NIR (K_s band in particular) data for ACs in other Local Group galaxies are needed to properly exploit the properties of the P–$W(V, K_s)$ relation.

ACKNOWLEDGEMENTS

We thank our anonymous referee for his/her very helpful comments that helped in improving the paper. VR warmly thanks Roberto Molinaro for providing the program for the spline interpolation of the light curves. We thank K. Bekki and R. Guandalini for helpful discussions. Partial financial support for this work was provided by PRIN-INAF 2011 (P.I. Marcella Marconi) and PRIN MIUR 2011 (P.I. F. Matteucci). We thank the UK's VISTA Data Flow System comprising the VISTA pipeline at the Cambridge Astronomy Survey Unit (CASU) and the VISTA Science Archive at Wide Field Astronomy Unit (Edinburgh) (WFAU) for providing calibrated data products supported by the STFC. RdG acknowledges research support from the National Natural Science Foundation of China (NSFC) through grant 11073001.

REFERENCES

Bekki K., Chiba M., 2007, MNRAS, 381, L16
Bersier D., 2000, ApJ, 534, L23
Bersier D., Wood P. R., 2002, AJ, 123, 840
Bessell M. S., Brett J. M., 1988, PASP, 100, 1134
Brocato E., Caputo F., Castellani V., Marconi M., Musella I., 2004, AJ, 128, 1597
Buonanno R., Corsi C. E., Castellani M., Marconi G., Fusi Pecci F., Zinn R., 1999, AJ, 118, 1671
Caputo F., 1998, A&AR, 9, 33
Caputo F., Marconi M., Musella I., 2000, A&A, 354, 610
Caputo F., Castellani V., Degl'Innocenti S., Fiorentino G., Marconi M., 2004, A&A, 424, 927
Carpenter J. M., 2001, AJ, 121, 2851
Cioni M.-R. L. et al., 2011, A&A, 527, 116 (Paper I)
Clementini G., Gratton R., Bragaglia A., Carretta E., Di Fabrizio L., Maio M., 2003, AJ, 125, 1309
Clementini G., Cignoni M., Contreras Ramos R., Federici L., Ripepi V., Marconi M., Tosi M., Musella I., 2012, ApJ, 756, 108
Cross N. J. G. et al., 2012, A&A, 548, A119
Dalton G. B. et al., 2006, in McLean I. S., Iye M., eds, Proc. SPIE Conf. Ser. Vol. 6269, Ground-based and Airborne Instrumentation for Astronomy. SPIE, Bellingham, p. 62690X
de Grijs R., 2011, An Introduction to Distance Measurement in Astronomy. Wiley, New York
Emerson J. P. et al., 2004, Proc. SPIE, 5493, 401
Emerson J. P., McPherson A., Sutherland W., 2006, The Messenger, 126, 41
Fiorentino G., Monelli M., 2012, A&A, 540, A102
For B.-Q., Staveley-Smith L., McClure-Griffiths N. M., 2013, ApJ, 764, 74
Freedman W. L. et al., 2001, ApJ, 553, 47
Gallart C., Aparicio A., Freedman W. L., Madore B. F., Martínez-Delgado D., Stetson P. B., 2004, AJ, 127, 1486
Greco C. et al., 2005, preprint (astro-ph/0507244)
Greco C. et al., 2009, ApJ, 701, 1323
Gullieuszik M., Held E. V., Rizzi L., Saviane I., Momani Y., Ortolani S., 2007, A&A, 467, 1025
Harris J., Zaritsky D., 2004, AJ, 127, 1531
Harris J., Zaritsky D., 2009, AJ, 138, 1243
Haschke R., Grebel E. K., Duffau S., 2011, AJ, 141, 158
Held E. V., Saviane I., Momany Y., 1999, A&A, 345, 747
Hidalgo S. L., Aparicio A., Martínez-Delgado D., Gallart C., 2009, ApJ, 705, 704
Holtzman J. A., Smith G. H., Grillmair C., 2000, AJ, 120, 3060
Irwin M. J. et al., 2004, Proc. SPIE, 5493, 411
Irwin M. J. et al., 2007, ApJ, 656, L13
Lindegren L., 2010, in Klioner S., Seidelmann P. K., Soffel M., eds, Proc. IAU Symp. 261, Relativity in Fundamental Astronomy: Dynamics, Reference Frames, and Data Analysis. Cambridge Univ. Press, Cambridge, p. 296
Lindegren L., Perryman M. A. C., 1996, Ap&SS, 116, 579
Madore B. F., 1982, ApJ, 253, 575
Madore B. F., Freedman W., 1991, PASP, 103, 933
Marconi M., Fiorentino G., Caputo F., 2004, A&A, 417, 1101
Marconi M., Musella I., Fiorentino G., 2005, ApJ, 632, 590
Martínez-Delgado D., Gallart C., Aparicio A., 1999, AJ, 118, 862
Matteucci A., Ripepi V., Brocato E., Castellani V., 2002, A&A, 387, 861
Menzies J., Feast M., Whitelock P., Olivier E., Matsunaga N., da Costa G., 2008, MNRAS, 385, 1045
Moretti M. I. et al., 2013, MNRAS, preprint (arXiv:1310.6849)
Muller E., Stanimirović S., Rosolowsky E., Staveley-Smith L., 2004, ApJ, 616, 845
Neilson H. R., Langer N., 2012, A&A, 537, 26
Pietrzyński G., Gieren W., Udalski A., 2003, AJ, 125, 2494
Pietrzyński G., Górski M., Gieren W., Ivanov V. D., Bresolin F., Kudritzki R.-P., 2009, AJ, 138, 459
Pietrzyński G. et al., 2013, Nature, 495, 76
Pritzl B. J., Armandroff T. E., Jacoby G. H., Da Costa G. S., 2002, AJ, 124, 1464
Putman M. E. et al., 1998, Nature, 394, 752
Riess A. et al., 2011, ApJ, 730, 119
Ripepi V., Moretti M. I., Clementini G., Marconi M., Cioni M.-R. L., Marquette J. B., Tisserand P., 2012a, Ap&SS, 341, 51
Ripepi V. et al., 2012b, MNRAS, 424, 1807
Rizzi L., Bresolin F., Kudritzki R. P., Gieren W., Pietrzyński G., 2006, ApJ, 638, 766
Soszyński I. et al., 2008, Acta Astron., 58, 293
Soszyński I. et al., 2012, Acta Astron., 62, 219
Stanimirović S., Staveley-Smith L., Jones P. A., 2004, ApJ, 604, 176
van der Marel R. P., Cioni M.-R. L., 2001, AJ, 122, 1807
Venzmer M. S., Kerp J., Kalberla P. M. W., 2012, A&A, 547, A12
Walker A., 2012, Ap&SS, 341, 43
Weisz D. R. et al., 2012, ApJ, 748, 88

SUPPORTING INFORMATION

Additional Supporting Information may be found in the online version of this article:

Table 3. K_s time series photometry of the ACs. (http://mnras.oxfordjournals.org/lookup/suppl/doi:10.1093/mnras/stt2047/-/DC1).

Please note: Oxford University Press are not responsible for the content or functionality of any supporting materials supplied by the authors. Any queries (other than missing material) should be directed to the corresponding author for the article.

This paper has been typeset from a TEX/LATEX file prepared by the author.